

1           **Investigation of the effect of DC electric field on a small ethanol diffusion flame**

2  
3                           Yanlai Luo <sup>1</sup>, Yunhua Gan <sup>1,\*</sup>, Xi Jiang <sup>2,\*\*</sup>

4  
5   1. School of Electric Power, South China University of Technology, Guangdong 510640, China;

6   2. Engineering Department, Lancaster University, Lancaster LA 1 4YR, UK

7  
8  
9                           **Submitted for publication in**

10  
11                           *Fuel*

12  
13  
14  
15   \*Corresponding author: Prof. Yunhua Gan, Ph.D.,

16   Address: School of Electric Power, South China University of Technology, Wushan Road, Tianhe

17   District, Guangzhou 510640, China

18   Tel/Fax: 00-86-20-87110613

19   Email: [ganyh@scut.edu.cn](mailto:ganyh@scut.edu.cn).

20  
21   \*\*Corresponding author: Prof. Xi Jiang, Ph.D.,

22   Address: Engineering Department, Lancaster University, Lancaster LA 1 4YR, UK

23   Tel/Fax: 00-44-1524592439

24   Email: [x.jiang@lancaster.ac.uk](mailto:x.jiang@lancaster.ac.uk).

1 **ABSTRACT**

2 A small ethanol diffusion flame exhibited interesting characteristics under a DC electric field. A  
3 numerical study has been performed to elucidate the experimental observations. The flow velocity,  
4 chemical reaction rate, species mass fraction distribution, flame deformation and temperature of the  
5 flame in the applied DC electric field were considered. The results show that the applied electric field  
6 changes the flame characteristics mainly due to the body forces acting on charged particles in the  
7 electric field. The charged particles are accelerated in the applied electric field, resulting in the flow  
8 velocity increase. The effects on the species distribution are also discussed. It was found that the  
9 applied electric field promotes the fuel/oxidizer mixing, thereby enhancing the combustion process  
10 and leading to higher flame temperature. Flame becomes shorter with applied electric field and its  
11 deformation is related to the electric field strength. The study showed that it is feasible to use an  
12 applied DC electric field to control combustion and flame in small-scale.

13

14 **Keywords:** Ethanol-air flame; DC electric field; micro-combustion; Numerical analysis; Flame  
15 deformation

## 1 Nomenclature

2

$c_p$  constant-pressure specific heat capacity

$D$  diffusivity

$d_i$  inner diameter of burner nozzle

$d_o$  outer diameter of burner nozzle

$E$  electric field strength

$e$  electron charge

$F$  body force

$H$  height of flame

$h_i$  enthalpy of species  $i$

$J_i$  diffusive flux of species  $i$

$k$  effective heat transfer coefficient

$L$  electrode spacing

$n_c$  net charge density

$n_+$  positive charge density

$n_-$  negative charge density

$p$  pressure on the element

$r$  radial direction

$R$  correlation coefficient

$R_e$  radius of electrode

$R_i$  net reaction rate of species  $i$

$S_h$	volume heat source term
$S_i$	additional generation rate caused by source terms
$T$	flame temperature
$u$	axial ( $x$ ) direction of flow velocity
$v$	radial ( $r$ ) direction of flow velocity
$W$	width of flame
$Y_i$	mass fraction of species $i$

### **Greek Letters**

$\alpha$	aspect ratio
$\mu$	dynamic viscosity
$\rho$	density of liquid ethanol
$\tau$	viscous dissipation stress

## 1 **1. Introduction**

2 The characteristics of micro- and meso-scale combustors with different configurations or under  
3 different external conditions have attracted lots of attention, e.g. [1-5]. The effects of an electric field  
4 applied on flame have been studied recently, e.g. [6-9]. Researchers found that the electric field can  
5 improve the stability of combustion. The external electric field was also used as a means for flame  
6 control, such as taking flame as an electrically active component based on voltage-current  
7 characteristics in the circuit [10]. The effects of electric fields on flame included stabilizing the  
8 combustion, increasing flame speed, reducing the soot production and emission, changing the flame  
9 temperature and shape [11-15]. These findings also imply that the efficiency of practical  
10 non-premixed combustion systems could be improved by applying an electric field [16]. It has been  
11 identified that there are three major effects produced by the electric field on the flame, including the  
12 thermal effect, the ionic wind effect and the electrical-chemical effect [17].

13 Experimental and numerical methods have been used to study the effects of electric fields on  
14 flame behavior. Meng et al. [18] found that the flame propagation and combustion properties were  
15 significantly affected by the DC electric fields and the flame shape would become a prolate spheroid  
16 by the electric body force in the electric field. Imamura et al. [19, 20] investigated the flame  
17 deformation of ethanol droplets in different vertical electric fields experimentally and the relation  
18 between the applied voltage and electrode distance was observed. Kim et al. [21] considered the  
19 stabilization characteristics of liftoff and blowoff in nonpremixed laminar jet flames in a coflow for  
20 propane fuel by applying AC and DC electric fields experimentally. Boom et al. [22] studied the  
21 influence of a DC electric field on the laminar burning velocity and found that the electrode  
22 configuration can influence the laminar burning velocities and the system requires a relatively low

1 power input. Belhi et al. [23] improved a simplified mathematical model, where negative ions and  
2 the stabilization mechanism of a diffusion lifted flame in the applied DC or AC electric fields were  
3 analyzed. The effects of electric fields on the reattachment of lifted flames have been investigated  
4 experimentally by Won et al. [24] and they reported that the stabilization limit of attached flames was  
5 extended by the AC electric field and the effect of DC was found to be minimal. Karnani and  
6 Dunn-Rankin [25] discussed the relationship among flame shape, combustion intensity, soot  
7 formation, and the ion production rate. They found that those parameters are related to the  
8 voltage–current relationship for a coflowing non-premixed methane/air flame. Vega et al. [26]  
9 studied the electro-physical means of controlling the nitrogen oxide pollutant formation and emission  
10 composition of premixed flames in the combustion process.

11 Most of these studies considered hydrocarbon fuels, especially gaseous fuels. Although  
12 diffusion flames with liquid fuels are important in terms of the effects of electric fields on  
13 combustion phenomena, the investigation is limited in the literature and there is still a lack of  
14 understanding on this topic. A small ethanol diffusion flame with an applied electric field was  
15 investigated in this study, investigating the effects of electrical field on combustion and the potential  
16 application in system control. The effects of DC electric field on the flame characteristics, such as  
17 flame shape, temperature, species distribution, flow velocity and reaction rate, were investigated  
18 experimentally and numerically. The combined experimental and numerical results enhance the  
19 understanding of the effects of electric field on the small ethanol diffusion flame. When small  
20 combustors are considered in transport applications such as a drone, liquid fuel is preferred because  
21 of the very large energy density (in comparison to gas fuels). The results and understandings  
22 obtained can be used to improve the performance of meso-scale combustors controlled using

1 electrical fields.

2

## 3 **2. Experiment**

### 4 2.1 Experimental system

5 The schematic of experimental apparatus and a simplified electrical circuit are shown in Fig. 1.

6 The system consists of four main parts, including liquid fuel supply system, small-scale combustion  
7 system, DC power supply system and measurement system. The fuel used in these experiments was  
8 high purity ethanol ( $C_2H_5OH$ , molecular weight of 46.07, purity > 99.5%) and it was controlled and  
9 supplied from the base into the burner nozzle with an inner diameter ( $d_i$ ) of 0.9 mm and outer  
10 diameter ( $d_o$ ) of 1.2 mm by a syringe pump (KDS 100) with an uncertainty of 1.0%. Air around the  
11 burner nozzle as the oxidizer was supplied from the ambient. The flame was ignited near the nozzle  
12 outlet and was located between two parallel horizontal brass plate electrodes with radius ( $R_e$ ) of 40  
13 mm. A potential difference applied by a DC power supply (Boher HV, Model 71030P) between the  
14 two electrodes produced the DC electric field. The measurement system consisted of digital camera  
15 (Cannon, EOS 5D Mark III) to observe the flame shape, S type platinum-rhodium thermocouple  
16 with the node diameter of 0.3 mm, and data acquisition instrument (Agilent, 34970A) to measure the  
17 flame temperature, which also could collect data of current and voltage. The system is similar to that  
18 used in our previous work [27-29].

19

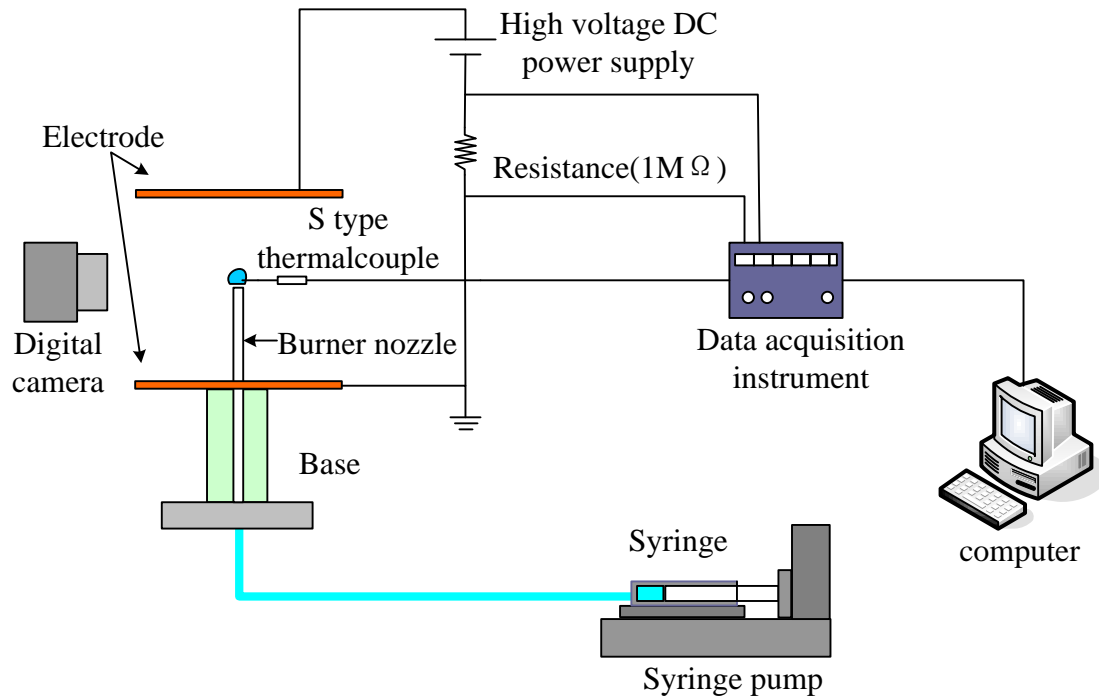


Fig. 1 Experimental system

## 2.2 Experimental method

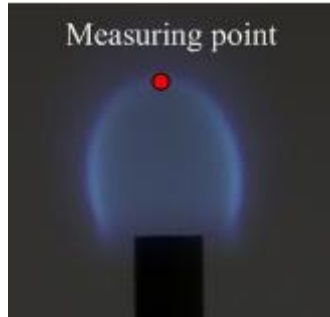
The applied voltage, normalized electrode spacing  $L$ , the nominal electric field strength ( $E$ ) are the key electrical parameters to describe the system. A positive electric field is defined as electric field vectors directed from the burner to the downstream electrode and reversely negative. When the power supply voltage or electrode distance was changed, the electric field strength would change accordingly and some different electric field conditions were produced. A small-scale diffusion flame in different electric field conditions was observed and the data such as flame shape, temperature variation and flow velocity were collected. These cases were compared and analyzed, and the effects of DC field on small-scale diffusion flame combustion characteristics were examined.

A thermocouple was used to measure the flame temperature at the flame top position, as shown in Fig. 2. The flame temperatures at different positions were measured and it was found that the highest temperature in the flame was at the top position. So the temperature at the top position was chosen to



1 represent the flame temperature. Moreover, the measurement at the top position brought the smallest  
2 disturbance to the flame compared with other positions [28].

3



4

5 Fig. 2 Flame temperature measuring point

6

7

### 8 **3. Model description**

#### 9 3.1 Geometric and mathematical model

10 Fig. 3 shows a schematic of the axisymmetric model of the small-scale combustor with two plate  
11 electrodes. The model scale depended on the actual experimental system. In the experiments,  
12 electrode spacing had been adjusted to 40 mm. The upper electrode was connected to the high  
13 voltage of the power supply as the anode and the upper electrode was connected to the low voltage as  
14 the cathode. In consideration of the domain symmetry, a half of the cross-section of the domain was  
15 selected in the axisymmetric model to reduce the computational cost.

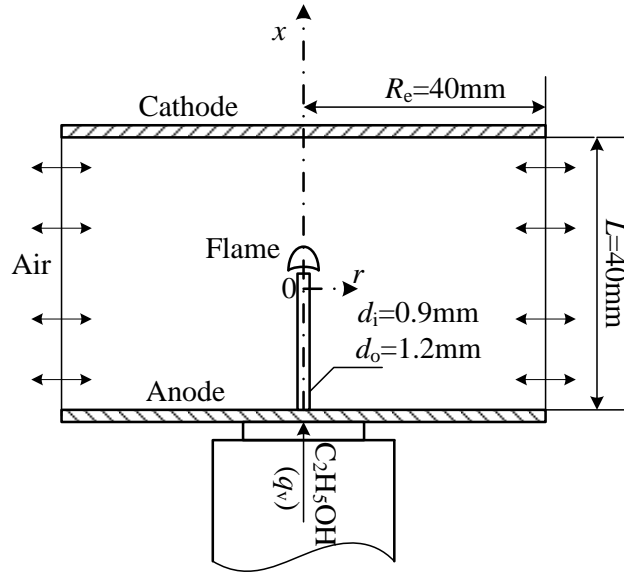


Fig. 3 The configuration studied

Since the main focus of the study was on the steady mean flow field, only steady and axisymmetric numerical simulations were considered. The mixture flow and combustion process followed conservation equations including the continuity, momentum, energy and species conservations for the governing equations.

In steady state, the governing equations of axisymmetric cylindrical coordinates are presented as follows:

Continuity:

$$\frac{\partial(\rho u)}{\partial x} + \frac{1}{r} \frac{\partial(r \rho v)}{\partial r} = 0 \quad (1)$$

where  $\rho$  is the density of flow,  $u$  is the  $x$  direction of flow velocity, and  $v$  is the  $r$  direction of flow velocity.

Momentum:

$x$  direction:

$$\frac{\partial(\rho uu)}{\partial x} + \frac{1}{r} \frac{\partial(r\rho uv)}{\partial r} = -\frac{\partial p}{\partial x} + 2\frac{\partial}{\partial x}(\mu \frac{\partial u}{\partial x}) + \frac{1}{r} \frac{\partial}{\partial r}(r\mu \frac{\partial u}{\partial r}) + \frac{1}{r} \frac{\partial}{\partial r}(r\mu \frac{\partial v}{\partial x}) + F_x \quad (2)$$

$r$  direction:

$$\frac{\partial(\rho uv)}{\partial x} + \frac{1}{r} \frac{\partial(r\rho vv)}{\partial r} = -\frac{\partial p}{\partial r} + \frac{\partial}{\partial x}(\mu \frac{\partial v}{\partial x}) + \frac{\partial}{\partial x}(\mu \frac{\partial u}{\partial r}) + \frac{2}{r} \frac{\partial}{\partial r}(r\mu \frac{\partial v}{\partial r}) + \frac{2\mu v}{r^2} + F_r \quad (3)$$

where  $\mu$  is the dynamic viscosity,  $p$  is the pressure on the flow element, and  $F_x, F_r$  are the body force on the element.

The source term of momentum equation in the axial direction is given as:

$$F_x = F_e = Ee(n_+ - n_-) = Een_c \quad (4)$$

where  $e$  is the electron charge,  $n_+$  is the positive charge density,  $n_-$  is the negative charge density, and  $n_c$  is the net charge density.

The model was simplified and the net charge density was considered. The number of charged particles was estimated according to the literature ( $10^9$ - $10^{12}$   $\text{cm}^{-3}$ ) [17-19]. According to Equation (4), the electric field force was estimated as

$$F = Een_c = 1600 \text{ N/m}^3, E=100 \text{ kV/m}, n_c=10^{11} \text{ cm}^{-3}$$

which is similar to the results in the literature (0-2000  $\text{N/m}^3$ ) [21].

Energy:

$$\frac{\partial}{\partial x}(\rho u h_i) + \frac{1}{r} \frac{\partial}{\partial r}(r\rho v h_i) = \frac{\partial}{\partial x}(\frac{k}{c_p} \frac{\partial h_i}{\partial x}) + \frac{1}{r} \frac{\partial}{\partial r}(r \frac{k}{c_p} \frac{\partial h_i}{\partial r}) - \frac{\partial(h_i \mathbf{J}_i)}{\partial x} - \frac{1}{r} \frac{\partial(h_i \mathbf{J}_i)}{\partial r} + \frac{\partial(\tau u)}{\partial x} + \frac{1}{r} \frac{\partial(r\tau v)}{\partial r} + S_h \quad (5)$$

where  $k$  is effective heat transfer coefficient,  $h_i$  is the enthalpy of the species  $i$ ,  $\mathbf{J}_i$  is the diffusive flux of the species  $i$ ,  $c_p$  is the constant-pressure specific heat capacity of the mixture, the temperature,  $\tau$  is the viscous dissipation stress, and  $S_h$  is the volumetric heat source term.

In our previous work [28], it was found that the external electric energy was very small compared with the actual burning thermal energy of ethanol in this study. This was also mentioned in the

1 reference [22]. So the external energy by the electric field was considered insignificant and ignored  
 2 in the model.

3 Species:

$$4 \quad \rho u \frac{\partial Y_i}{\partial x} + \rho v \frac{\partial Y_i}{\partial r} = -\frac{\partial J_i}{\partial x} - \frac{1}{r} \frac{\partial (r J_i)}{\partial r} + R_i + S_i \quad (6)$$

5 where  $Y_i$  is the mass fraction of species  $i$ ,  $R_i$  is the net reaction rate,  $S_i$  is the additional  
 6 generation rate caused by source terms.

7 In order to simplify the calculation, a one-step chemical reaction model was used.



9 The governing equations were solved using an implicit solver which is pressure based. The system  
 10 was closed with appropriate boundary conditions on each side of the computational domain. For the  
 11 small diffusion flame, the boundary conditions are consistent with the experimental condition, as  
 12 shown in Table 1. Identical boundary conditions were employed for the condition with electric field  
 13 and without electric field except for the electrode conditions. It was assumed that the purity of liquid  
 14 ethanol was 99.7%, the temperature of the liquid fuel applied was 300 K and the ethanol was  
 15 completely burnt. The model considered that the liquid ethanol had evaporated into gas near the  
 16 nozzle outlet. This is consistent with the actual experimental observation.

17 Table 1 Boundary conditions

Liquid ethanol inlet boundary condition	VELOCITY_INLET
Outlet boundary condition	PRESSURE_OUTLET
The wall of tube inside and outside	WALL
The electrodes condition	WALL

18

### 19 3.2 Numerical simulation and validation

20 The computational domain took the differences of the solid and the fluid zones into consideration,

1 which was divided into the ceramic tube solid zone, the fluid and combustion zone. A systematic grid  
2 independence test was carried out. The final mesh chosen had a total number of elements of 159980.  
3 Numerical simulations were performed for a reacting flow system with ethanol and air used as the  
4 fuel and oxidant respectively. In the simulation study, the oxygen mass fraction was taken as 23% (in  
5 ambient air). The ethanol was ignited above the burner nozzle outlet by assuming a temperature of  
6 1000 K.

7 The accuracy of the present numerical model has been evaluated by comparing the measured and  
8 predicted flame shape and temperature. The small flame image captured by camera in the experiment  
9 and the flame temperature distribution of numerical calculation are shown in Fig. 4, respectively.  
10 Generally, in the high temperature region, the brightness of the flame will be high. So the flame  
11 image captured by camera and the calculated temperature field could indirectly reflect the flame  
12 shape. It was found that the flame shapes obtained from the two approaches were similar, which  
13 were both approximately spherical. Through the comparison of the flame temperature measured and  
14 calculated data, the difference between them was about 9%, and it is shown in Table 2. This was  
15 considered as acceptable. In addition, when the operating condition changed, the flame and  
16 temperature obtained by the measured results and calculated results both have the same trend of  
17 variation. It also implied the accuracy of the present numerical simulation.

18

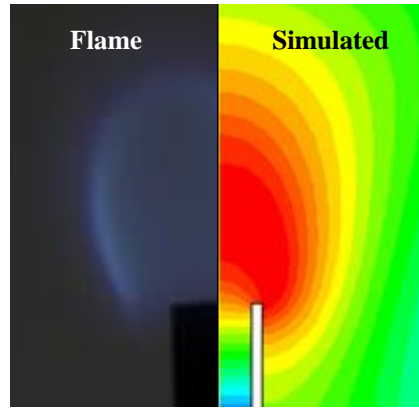


Fig. 4 Measured flame image and simulated temperature field without electric field ( $q_v=1.2$  ml/h)

Table 2 Flame temperature and errors with flow rate of 1.2 ml/h

Temperature/K	no electric field	electric field
Experimental data	1326	1388
Numerical data	1446	1472
Discrepancies	9.0%	6.1%

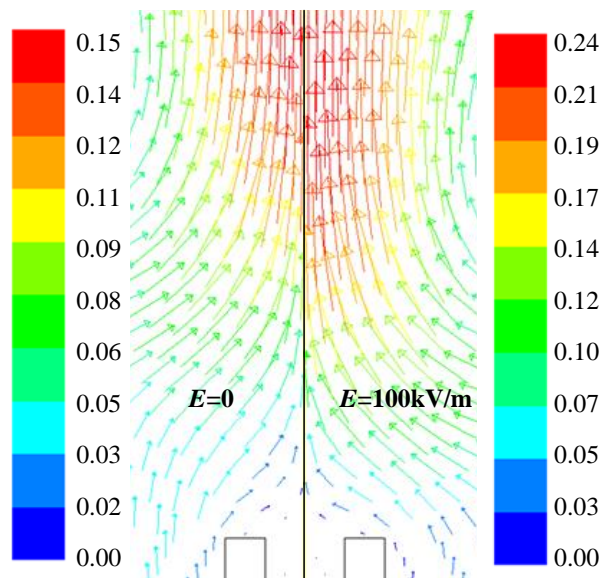
## 4. Results and discussion

### 4.1 Velocity field

The flame of liquid ethanol in our small-scale combustor can only maintain stability within a certain range of fuel flow rates. When the fuel flow rate is too low or too high, the small flame cannot be ignited or will become oscillatory. In this study, the flame in a steady state was examined. The fuel flow rate of 1.2 ml/h where the flame could maintain stability was selected to perform the studies. Results about flow field of the flame were obtained. Fig. 5 shows the flow velocity vector diagrams near the flame without electric field and under positive electric field. Fig. 6 shows the comparison of flow field variations without and with the applied electric field. It was found that the velocity magnitude increased and the velocity changed more intensely when the electric field was applied.

This is mainly due to the influence of ionic wind [23]. There is a large number of positively and

1 negatively charged particles being produced by chemi-ionization in the hydrocarbon flame reaction  
2 zone [30]. The positive electrode is below the flame and the negative electrode is above. These  
3 charged particles would affect the combustion progress when the DC electric field was applied.  
4 When the electric field was applied, the positively and negatively charged particles would move  
5 toward the opposite polarity electrode by the force of electric field. Charged ions accelerated in the  
6 electric field and transferred their momentum to the neutral molecules by colliding with them. With  
7 the relatively small mean free path, the ions were accelerated by the electric field after each collision  
8 [31], which produced a large number of neutral molecules moving toward the electrodes. The net  
9 effect of this process is a significant body force produced by the electric field or the so-called “ionic  
10 wind”. In the same region, the flow velocity near the flame changed more intensely under the electric  
11 field compared with the case without the electric field. It suggested that the velocity gradient is larger,  
12 which also indicated the existence of the electric field force as a source for the momentum [21].



13  
14 Fig. 5 Calculated velocity field for the diffusion flame. Left: no electric field, right:  $E=100\text{ kV/m}$   
15  $(q_v=1.2\text{ ml/h})$   
16

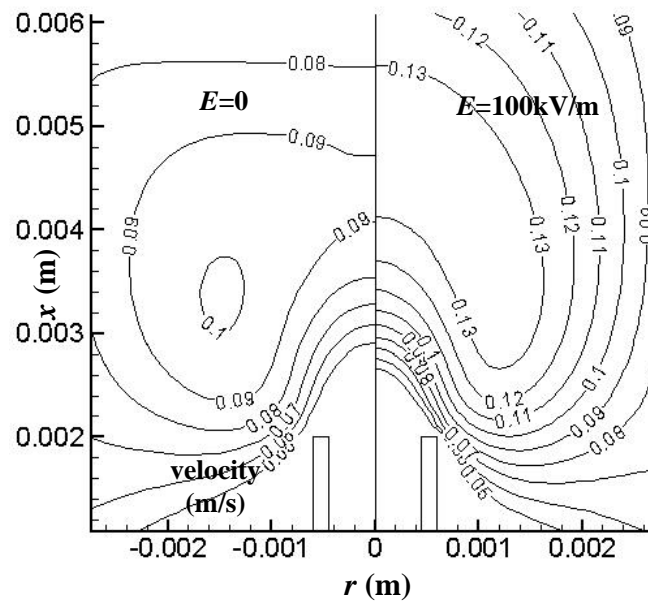


Fig. 6 Calculated velocity contour. Left: no electric field, right:  $E=100\text{ kV/m}$  ( $q_v=1.2\text{ ml/h}$ )

#### 4.2 Mass fraction distribution

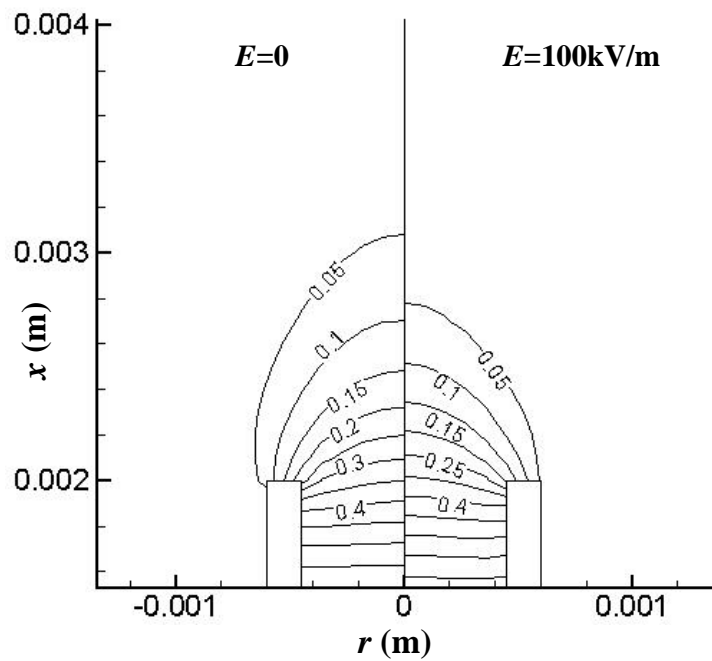
Obtained by numerical simulations, Fig. 7 and Fig. 8 show the ethanol and  $\text{CO}_2$  mass fraction distributions, respectively. The effects of applied electric field on the species distribution can be observed. As seen from the figures, when the DC electric field was applied, the concentration of each species has a tendency of inward contraction. The increasing flow velocity near the flame due to the addition of electric field enhances the mixing of species. The applied electric field could increase the flame propagation velocity [18] and flame temperature by increasing the ion number density and redistributing the ion concentration, which enhances the combustion. The fuel rapidly spread to the air and met the oxidant and then the reaction took place. The fuel and oxidant burnt faster and were quickly consumed. The intensity of combustion process increased, and species distribution had an inward contraction.

A similar phenomenon can be seen from the calculated mass fraction profiles of  $\text{O}_2$  and  $\text{CO}_2$  on the axis as shown in Fig. 9. The maximum value of the mass fraction of  $\text{CO}_2$  under positive electric field



1 was a little higher than that without the electric field and the point of maximum value moved  
2 upstream. The mass fraction of  $O_2$  also moved upstream and became more sharply decreasing close  
3 to the flame. This observation agreed with the experimental results, which showed the reduction of  
4 flame height with the increasing electric field strength. These results showed that the flame had a  
5 tendency of contraction, which also implied the intensification of the reaction.

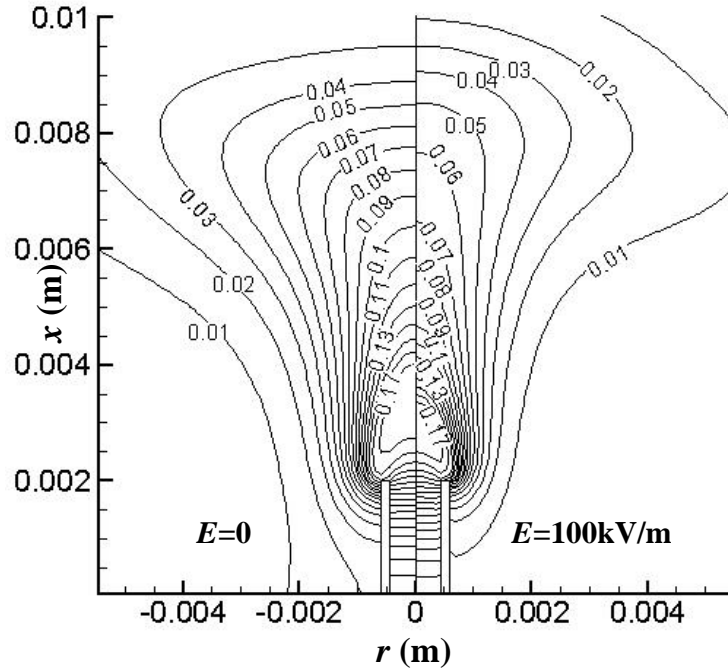
6



7

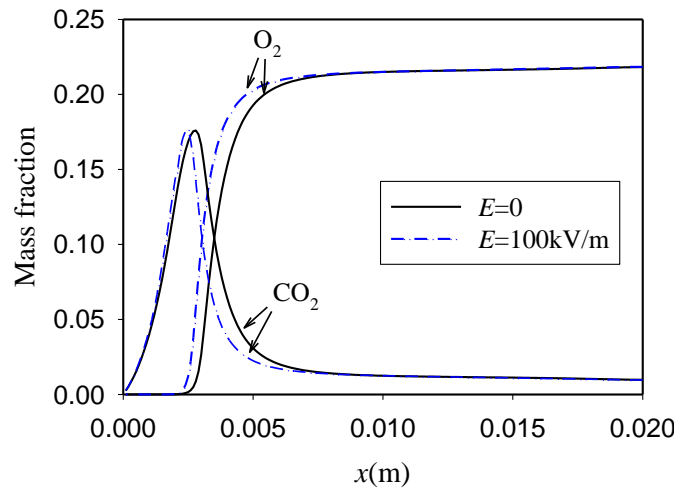
8 Fig. 7 Calculated ethanol mass fraction. Left: no electric field, right:  $E=100\text{ kV/m}$  ( $q_v=1.2\text{ ml/h}$ )

9



1  
2

Fig. 8 Calculated CO<sub>2</sub> mass fraction. Left: no electric field, right:  $E= 100\text{ kV/m}$  ( $q_v=1.2\text{ ml/h}$ )



3  
4

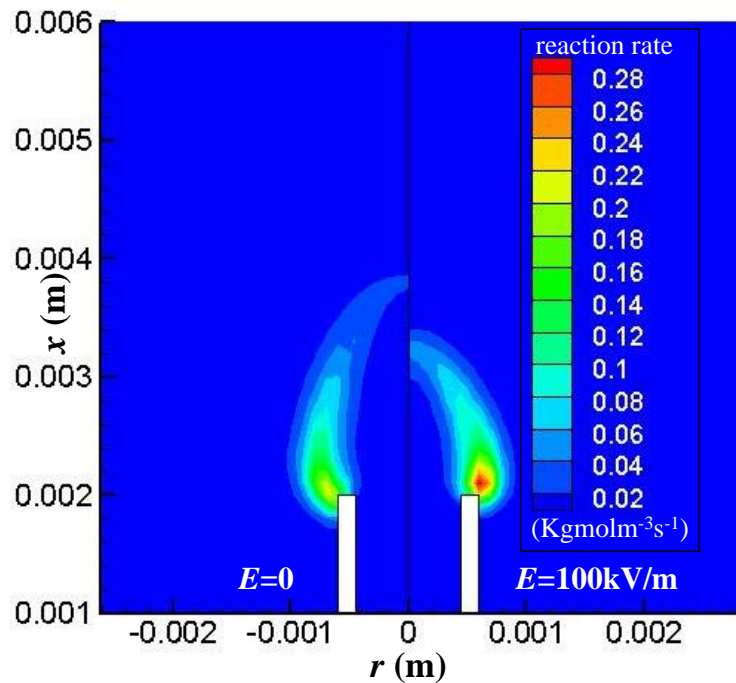
Fig. 9 Calculated mass fraction profiles of O<sub>2</sub> and CO<sub>2</sub> on the axis ( $q_v=1.2\text{ ml/h}$ )

5  
6

### 4.3 Chemical reaction rate

7 From the numerical results, some changes in chemical reaction were observed when the electric  
8 field was applied. Fig. 10 shows the chemical reaction rate in the flame. It can be found that when  
9 the electric field was applied, the reaction rate in the flame increased and the scope of the reaction  
10 expanded slightly. While the surface of chemical reactions has a tendency of contraction, which is

1 consistent with the mass fraction discussed before. It also suggests that the flame size decreases. It is  
 2 known from the above that velocity close to the increased, which enhanced the fuel/oxygen mixing.  
 3 The charged particles received an acceleration by electric field, which made charged particles mix  
 4 quickly with oxygen in the flame front [10] and the reaction took place in a wider space. Thus, the  
 5 reaction rate increased resulting in the fuel burning faster and the inward contraction of the flame  
 6 front to the fuel side. It means that the DC electric field can enhance the combustion process and in  
 7 turn lead to a higher flame temperature.

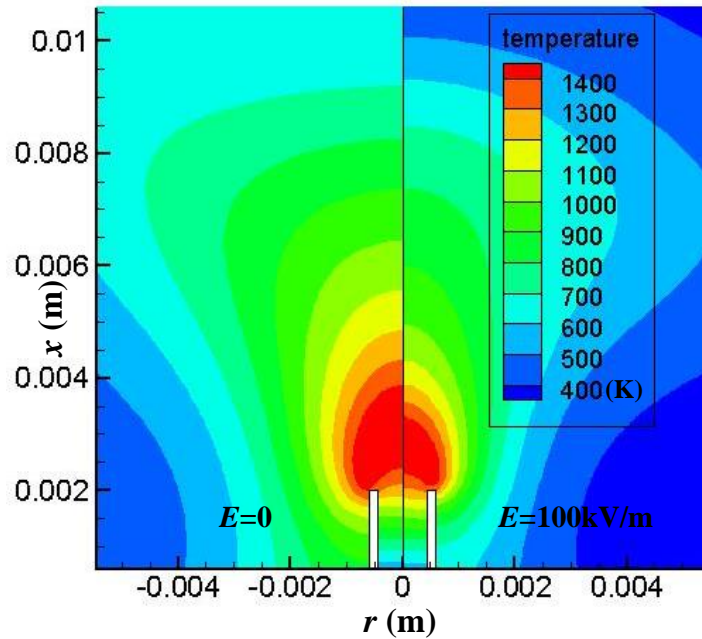


8  
 9 Fig. 10 Chemical reaction rate. Left: no electric field, right:  $E= 100 \text{ kV/m}$  ( $q_v=1.2 \text{ ml/h}$ )

#### 11 4.4 Flame deformation in electric field

12 One important characteristic of laminar diffusion flame is the flame shape or structure. Fig. 11  
 13 shows the calculated temperature distribution of flame without electric field condition (left) and that  
 14 under positive electric field (right) which also reflects the flame shape. Fuel flow rate was 1.2 ml/h,  
 15 and the applied voltage was 4.0 kV ( $E=100 \text{ kV/m}$ ). It shows that the flame became shorter and

1 smaller after the electric field was applied. The flame height decreased by 50% with an applied  
 2 electric field.



3  
 4 Fig. 11 Calculated temperature fields. Left: no electric field, right:  $E= 100 \text{ kV/m}$  ( $q_v=1.2 \text{ ml/h}$ )

5  
 6 The maximum temperature with electric field appeared to be 1472 K which was slightly above (by  
 7 4.7%) the temperature with no electric field (1446 K). Owing to these aerodynamic effects associated  
 8 with the electrical field, the entire flow field is affected, and in particular the flame shape, which is  
 9 well known to be very sensitive to the surrounding flow field [32], is influenced accordingly. Thus,  
 10 the flame scale became smaller.

11 The aspect ratio was defined as the ratio of the flame height ( $H$ ) to width ( $W$ )

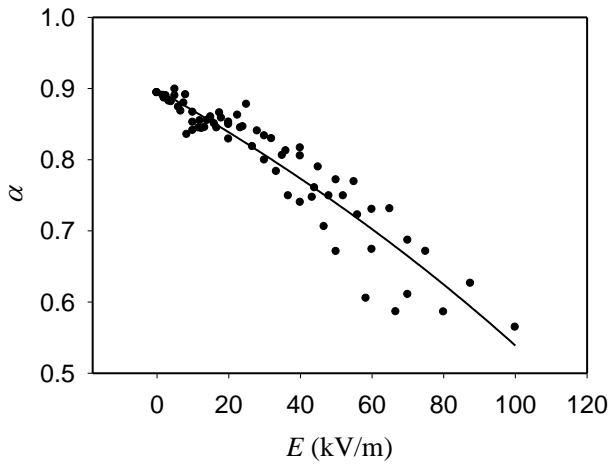
$$\alpha = H/W \tag{8}$$

13 Fig. 12 shows the changes of flame deformation rate with the applied DC electric field strength  
 14 obtained from the experimental results. The results show a satisfactory correlation with the best fit of  
 15 the following equation with correlation coefficient  $R=0.9408$ .

$$\alpha = \frac{0.8983 - 0.0047E}{1 - 0.002E} \quad (9)$$

1 It could be found that the flame deformation rate became smaller with the increasing electric field  
 2 strength. When the electric field strength was stronger, the electric field force was greater and the  
 3 flame became flatter.  
 4

5 The flame shape is affected by the surrounding flow field, reaction rate and diffusion. The height  
 6 of the laminar diffusion flame is proportional to the fuel flow rate, and is inversely proportional to  
 7 the diffusion coefficient  $D$ . As known from the Fick's Diffusion Law,  $D$  is nearly proportional to  
 8  $T^{3/2}$ . According to the results of flame temperatures and discussions above, the flame temperature  
 9 with applied electric field is higher than that without electric field. So the diffusivity increased and  
 10 the flame became shorter under the effect of DC electric field. The electric field increased the flow  
 11 velocity by the electric force and promoted the reaction rate and the diffusion of the species which  
 12 also made the flame length shorter.



13  
 14 Fig. 12 The flame deformation rate with electric field strength collecting by experimental results  
 15 ( $q_v=1.2$  ml/h)  
 16

17 **5. Conclusions**

1 The effects of DC electric field on the small ethanol diffusion flame were investigated. The flow  
2 velocity, chemical reaction rate, mass fraction distribution, flame temperature and deformation in the  
3 applied DC electric field were considered. The results show that the applied electric field changes the  
4 flame characteristics mainly due to the body forces acting on charged particles. The applied electric  
5 field accelerates the charged particles and they collide with the neutral particles and transfer the  
6 momentum, thus increasing the flow velocity. The effects on the species distribution and the flow  
7 field near the flame by the applied electric field promote the mixing of fuel and oxidant, which  
8 enhances the combustion process and leads to higher flame temperature. Flame becomes shorter with  
9 applied electric field and its deformation is related to the electric field strength.

10

## 11 **Acknowledgements**

12 The authors gratefully acknowledge the National Natural Science Foundation of China (51376066,  
13 51611130194), State Key Laboratory of Engines of Tianjing University (K2016-01) of China and the  
14 Royal Society-Newton Mobility Grant of the United Kingdom (IE151100).

15

## 16 **References**

- 17 [1] Ju Y, Maruta K. Microscale combustion: Technology development and fundamental research.  
18 *Prog Energy Combust Sci* 2011; 37(6): 669-715.
- 19 [2] Jun L, Yuantao W, Junrui S, Xueling L. Dynamic behaviors of premixed hydrogen-air flames in a  
20 planar micro-combustor filled with porous medium. *Fuel* 2015; 145: 70-78.
- 21 [3] Li J, Chou SK, Li ZW, Yang WM. Experimental investigation of porous media combustion in a  
22 planar micro-combustor. *Fuel* 2010; 89(3): 708-715.

- 1 [4] Gan YH, Luo ZB, Cheng YP, Xu JL. The electro-spraying characteristics of ethanol for  
2 application in a small-scale combustor under combined electric field. *Appl Therm Eng* 2015; 87:  
3 595-604.
- 4 [5] Bagheri G, Hosseini SE, Wahid MA. Effects of bluff body shape on the flame stability in  
5 premixed micro-combustion of hydrogen–air mixture. *Appl Therm Eng* 2014; 67(1-2): 266-272.
- 6 [6] Tomcik P, Klaus P, Kulhanek J, Trojan R. Influence of electric field on stabilization of flame from  
7 poor methane-oxygen mixture. *IEEE T Plasma Sci* 2013; 41(8): 2230-2236.
- 8 [7] Maricq MM. The dynamics of electrically charged soot particles in a premixed ethylene flame.  
9 *Combust Flame* 2005; 141(4): 406-416.
- 10 [8] Maricq MM. Size and charge of soot particles in rich premixed ethylene flames. *Combust Flame*  
11 2004; 137(3): 340-350.
- 12 [9] Xu KG. Plasma sheath behavior and ionic wind effect in electric field modified flames. *Combust*  
13 *Flame* 2014; 161(6): 1678-1686.
- 14 [10] Borgatelli F, Dunn-Rankin D. Behavior of a small diffusion flame as an electrically active  
15 component in a high-voltage circuit. *Combust Flame* 2012; 159(1): 210-220.
- 16 [11] Dae Geun P, Byung Chul C, Min Suk C, Suk Ho C. Soot reduction under DC electric fields in  
17 counterflow non-premixed laminar ethylene flames. *Combust Sci Technol* 2014; 186(4-5): 644-656.
- 18 [12] Wisman DL, Marcum SD, Ganguly BN. Electrical control of the thermodiffusive instability in  
19 premixed propane-air flames. *Combust Flame* 2007; 151(4): 639-648.
- 20 [13] Sakhrieh A, Lins G, Dinkelacker F, Hammer T, Leipertz A, Branston DW. The influence of  
21 pressure on the control of premixed turbulent flames using an electric field. *Combust Flame* 2005;  
22 143(3): 313-322.

- 1 [14] Marcum SD, Ganguly BN. Electric-field-induced flame speed modification. *Combust Flame*  
2 2005; 143(1-2): 27-36.
- 3 [15] Ata A, Cowart JS, Vranos A, Cetegen BM. Effects of direct current electric field on the blowoff  
4 characteristics of bluff-body stabilized conical premixed flames. *Combust Sci Technol* 2005; 177(7):  
5 1291-1304.
- 6 [16] Giorgi MGD, Sciolti A, Campilongo S, Pescini E, Ficarella A, Martini LM, Tosi P, Dilecce G.  
7 Plasma assisted flame stabilization in a non-premixed lean burner. *Energy Procedia* 2015; 82:  
8 410-416.
- 9 [17] Zhang Y, Wu YX, Yang HR, Zhang H, Zhu M. Effect of high-frequency alternating electric  
10 fields on the behavior and nitric oxide emission of laminar non-premixed flames. *Fuel* 2013; 109:  
11 350-355.
- 12 [18] Meng XW, Wu XM, Kang C, Tang AD, Gao ZQ. Effects of Direct-Current (DC) electric fields  
13 on flame propagation and combustion characteristics of premixed CH<sub>4</sub>/O<sub>2</sub>/N<sub>2</sub> flames. *Energy Fuels*  
14 2012; 26(11): 6612-6620.
- 15 [19] Imamura O, Chen B, Nishida S, Yamashita K, Tsue M, Kono M. Combustion of ethanol fuel  
16 droplet in vertical direct current electric field. *Proc Combust Inst* 2011; 33(2): 2005-2011.
- 17 [20] Imamura O, Yamashita K, Nishida S, Ianus G, Tsue M, Kono M. Two-droplet combustion of  
18 n-octane in a direct current electric field under microgravity. *Combust Sci Technol* 2011; 183(8):  
19 755-763.
- 20 [21] Kim MK, Ryu SK, Won SH, Chung SH. Electric fields effect on liftoff and blowoff of  
21 nonpremixed laminar jet flames in a coflow. *Combust Flame* 2010; 157(1): 17-24.
- 22 [22] van den Boom JDBJ, Konnov AA, Verhasselt AMHH, Kornilov VN, de Goey LPH, Nijmeijer H.



- 1 The effect of a DC electric field on the laminar burning velocity of premixed methane/air flames.  
2 Proc Combust Inst 2009; 32(1): 1237-1244.
- 3 [23] Belhi M, Domingo P, Vervisch P. Modelling of the effect of DC and AC electric fields on the  
4 stability of a lifted diffusion methane/air flame. Combust Theor Model 2013; 17(4): 749-787.
- 5 [24] Won SH, Cha MS, Park CS, Chung SH. Effect of electric fields on reattachment and  
6 propagation speed of tribrachial flames in laminar coflow jets. Proc Combust Inst 2007; 31: 963-970.
- 7 [25] Karnani S, Dunn-Rankin D. Detailed characterization of DC electric field effects on small  
8 non-premixed flames. Combust Flame 2015; 162(7): 2865-2872.
- 9 [26] Vega EV, Shin SS, Lee KY. NO emission of oxygen-enriched CH<sub>4</sub>/O<sub>2</sub>/N<sub>2</sub> premixed flames under  
10 electric field. Fuel 2007; 86(4): 512-519.
- 11 [27] Gan YH, Xu JL, Yan YY, Wang M, Luo YL, Yang ZL. A comparative study on free jet and  
12 confined jet diffusion flames of liquid ethanol from small nozzles. Combust Sci Technol 2014;  
13 186(2): 120-138.
- 14 [28] Gan YH, Wang M, Luo YL, Chen XW, Xu JL. Effects of direct-current electric fields on flame  
15 shape and combustion characteristics of ethanol in small scale. Adv Mech Eng 2016; 8(1): 1-14.
- 16 [29] Gan YH, Luo YL, Wang M, Shi YL, Yan YY. Effect of alternating electric fields on the  
17 behaviour of small-scale laminar diffusion flames. Appl Therm Eng 2015; 89: 306-315.
- 18 [30] Weinberg FJ, Dunn-Rankin D, Carleton FB, Karnani S, Markides C, Zhai M. Electrical aspects  
19 of flame quenching. Proc Combust Inst 2013; 34: 3295-3301.
- 20 [31] Lawton J, Weinberg FJ, electrical aspects of combustion, Clarendon Press, Oxford, 1969.
- 21 [32] Hu J, Rivin B, Sher E. The effect of an electric field on the shape of co-flowing and candle-type  
22 methane-air flames. Exp Therm Fluid Sci 2000; 21(1-3): 124-133.

1 **List of figure captions**

2 Fig. 1 Experimental system

3 Fig. 2 Flame temperature measuring point

4 Fig. 3 The configuration studied

5 Fig. 4 Measured flame image and simulated temperature field without electric field ( $q_v=1.2$  ml/h)

6 Fig. 5 Calculated velocity field for the diffusion flame. Left: no electric field, right:  $E= 100$  kV/m  
7 ( $q_v=1.2$  ml/h)

8 Fig. 6 Calculated velocity contour. Left: no electric field, right:  $E= 100$  kV/m ( $q_v=1.2$  ml/h)

9 Fig. 7 Calculated ethanol mass fraction. Left: no electric field, right:  $E= 100$  kV/m ( $q_v=1.2$  ml/h)

10 Fig. 8 Calculated CO<sub>2</sub> mass fraction. Left: no electric field, right:  $E= 100$  kV/m ( $q_v=1.2$  ml/h)

11 Fig. 9 Calculated mass fraction profiles of O<sub>2</sub> and CO<sub>2</sub> on the axis ( $q_v=1.2$  ml/h)

12 Fig. 10 Chemical reaction rate. Left: no electric field, right:  $E= 100$  kV/m ( $q_v=1.2$  ml/h)

13 Fig. 11 Calculated temperature fields. Left: no electric field, right:  $E= 100$  kV/m ( $q_v=1.2$  ml/h)

14 Fig. 12 The flame deformation rate with electric field strength collecting by experimental results  
15 ( $q_v=1.2$  ml/h)